Aerodynamic performance of tailored microparticles as carriers in dry powder inhaler formulations made by multi-focus multi-photon 3D laser printing

Check for updates

Melvin Wostry[1,5], Alexander Berkes [2,5], Pascal Kiefer[2], Martin Wegener [2,3] & Regina Scherließ [1,4] ✉
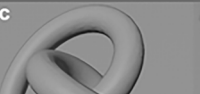
The influence of carrier particle's geometry on its performance as a drug carrier remains a challenge. Here, tailored and additively manufactured microparticles as carriers in interactive powder mixtures for inhalation are investigated. The crucial step of production of 50 μm sized complex microparticles is accomplished by multi-photon 3D laser printing. The produced powder is mixed with a model drug. Four different potential carrier geometries are printed, as well as three different surface roughnesses, created by altering the printing settings. All interactive powder mixtures are tested for drug homogeneity and aerodynamic performance, scouting for the carrier geometry with the highest drug fine particle fraction below 5 μm, i.e., the respirable fraction. A significant difference in the performance of the geometries is found, with one geometry, i.e., the Pharmacone, showing the best results. The surface roughness has no significant influence on the fine particle fraction during the aerodynamic assessment.

Pulmonary drug delivery is a favorable, commercially used route for drug administration, especially for locally treated diseases such as asthma and chronic obstructive pulmonary disease (COPD)[1,2]. Initially in pulmonary drug delivery, patients were treated with drug solutions given by inhaler devices such as nebulizers or pressurized metered dose inhalers (pMDIs). However, dry powder inhalation has gained significant market share and, in some countries, dominates inhalation therapy[3–5]. Nevertheless, the development of dry powder formulations has its own difficulties. After dispersion from the device particles passively follow the inhaled airstream through the airways[6,7]. Large particles tend to deposit in the throat or upper airways due to impaction. With further branching of the bronchi, the diameter becomes narrower while the number of airways increase leading to an overall increase of the cross-sectional area leading to a decrease in airstream velocity. In a low-velocity environment, drug particles that reach the tissue can deposit by sedimentation and diffusion. Particles that are too small and thus too light for sedimentation are unlikely to deposit and will be exhaled again. Therefore, an aerodynamic particle diameter between 1 and 5 μm is needed to ensure the drug is able to reach its therapeutic target[8,9]. The aerodynamic diameter is defined as the diameter of a spherical particle with the unit density of 1 g/cm^3 and the same settling velocity as the tested particle[10,11]. Micronised drugs of this size encounter challenges related to flowability and overall processability into a final dosage form. Especially the strong cohesion due to its large surface and contact areas leads to bad flowability of the powder bulk. A common strategy used in most commercially available medications to tackle this problem is the interactive powder mixture. The interactive powder mixture consists of at least two compounds: Firstly, the micronised drug and secondly a large fraction of coarse particles of an excipient material serving as carrier. In most cases α-lactose monohydrate with a particle diameter between 30 and 200 μm is used as carrier particle[12]. Drug and lactose are mixed, resulting in the micronised drug particles being attached to the surface of the carrier particle. With this, blend bulk characteristics are dominated by carrier properties and the processability of the powder blend is enhanced. During inhalation, mechanical forces in the inhalation air stream detach and disperse the attached drug particles as an inhalable aerosol[13]. Thus, the drug is separated from the carrier particle, the latter impacts in the oropharynx and is swallowed. As most commercial inhalation products aim for a local therapy, it is favorable to reduce the amount of not-detached, therefore swallowed and systemically active API,

[1]Department of Pharmaceutics and Biopharmaceutics, Kiel University, Gutenbergstraße 76, 24118 Kiel, Germany. [2]Institute of Applied Physics (APH), Karlsruhe Institute of Technology (KIT), Wolfgang-Gaede-Str. 1, 76131 Karlsruhe, Germany. [3]Institute of Nanotechnology (INT), Karlsruhe Institute of Technology (KIT), P.O. Box 3640, 76021 Karlsruhe, Germany. [4]Priority Research Area Kiel Nano, Surface and Interface Sciences (KiNSIS), Kiel University, Christian-Albrechts-Platz 4, 24118 Kiel, Germany. [5]These authors contributed equally: Melvin Wostry, Alexander Berkes. ✉e-mail: rscherliess@pharmazie.uni-kiel.de

Fig. 1 | Designs of the potential carrier particles.
a Soccerball, **b** Sphere, **c** Rollingknot, **d** Pharmacone with their respective surface area (A) and mass per particle (M), disregarding hatching and slicing.

which would come along with more side effects[14]. The digestion of the API reduces bioavailability in the lungs, which will be especially uneconomic for price-intensive therapeutics. The balanced interaction between carrier particle and drug is therefore a crucial aspect of the performance[15], which in this context means the successful delivery of active pharmaceutical ingredients (API) to the site of action, i.e., the lung tissue and the alveoli.

The lactose used for inhalation is of high quality; typically, sieved lactose crystals of narrow size distribution and varying degree of fines are utilized[16,17]. Despite their general similarity, lactose particles are not identical regarding shape and size. Aerosolization and movement of particles in the air flow is highly dependent on the particle shape. While inter- and intra-patient variability in inhalation patterns as well as the complex anatomy of the lung in combination with disease-related changes already lead to major challenges in drug delivery, exactly identical carrier particles could at least reduce one influencing factor on the drug product's side. This could hypothetically be one step towards the goal of a more homogeneous and replicable drug dispersion and drug administration to the patient. In terms of fundamental research, a uniform powder with precisely controlled and adjustable size and morphology could improve the statistical liability of experimental setups comparing for example different API or the influence of particle surface modifications such as the surface roughness due to the reduced number of influential factors[18,19].

By producing tailor-made carrier particles with a designed geometry, it can be investigated how carrier particles with certain geometries influence API availability in the lungs.

In the past, several approaches for producing particles for inhalation in a desired shape and size have been tested. Important to mention is the particle replication in non-wetting templates (PRINT) technology[20]. This method allowed for a large number of produced particles, nevertheless the complexity of such particles was limited by the production method. The template approach was dependent on at least one flat surface of the produced particle, furthermore, sharp edges such as surface spikes or hollow geometries were not accessible. Other methods, such as pollen- or flower-shaped[21,22] carrier particles created by controlled crystallization processes, allowed for more complex particle geometries but lacked control of a narrow particle size distribution and exact design of the particle shape.

Thus, to date, no production method has been described in the literature, that enables production of uniform and monodisperse carrier particles while, at the same time, imposing little to no limitations on particle geometry complexity. Here, our study introduces a hitherto unprecedented possibility of precise particle design and production.

Additive manufacturing is a new approach for preparing carrier particles below 100 µm in diameter[23]. In this context the overall most useful manufacturing technique to create particles of the desired complex shape and size is multi-photon 3D laser printing[23]. However, to obtain the necessary amount of carrier particles to conduct quantitative experiments assessing their performance, the manufacturing would quickly exceed years of print time due to the sequential mode of fabrication. Due to recent advancements in the field of fast 3D laser printing, such printing endeavors are now within reach[24]. By paralleling the printing process, 400,000 carrier particles with 50 µm diameter and sub-micrometer definition can be printed in less than 8 hours, enabling the manufacture of sufficient amounts to allow

experimental studies of various carrier particle properties on their performance.

These mass-produced particles consist of polymers, made by radical polymerization, and are not safe to be inhaled by humans, mostly due to possible residual photo initiator and the fact, that they are not degradable. Here, carrier particles produced by 3D laser printing are therefore only used to investigate the influence of geometry on carrier particle performance. Nevertheless, research for non-cytotoxic and possibly digestible photo resists, which could be mass-produced with multi-photon 3D laser printing, is ongoing[25]. Additionally, research on holographic multi-photon 3D laser nanoprinting is ongoing[26]. Such approaches potentially enable the manufacturing of tailored microparticles at rates that are several orders of magnitude faster than what we have used in the present article, thereby bringing actual pharmaceutical applications into reach.

Designing carrier particles should account for different properties required in the formulation. In the bulk powder, the API particles should adhere to the carrier particles in a uniform manner to allow homogeneous distribution of the API and shall impose adequate flowability to the bulk powder to ensure powder processability, filling and dosing. During inhalation, the formulation will allow dispersion and drug detachment to maximize targeting the lungs. The theoretical choice of geometries is endless[27], and computer simulation may be used to identify preferred structures[28,29]. Designing carrier particles also needs to consider the printability, which may exclude certain geometries such as structures with parts that are finer than the printing resolution.

In a prior study, the influence of a carrier particle's shape on its drug adhesion behavior was investigated[30]. The goal of this study was to design, print and experimentally test different morphologies as geometries for potential carrier particles for dry powder formulations. The perfectly symmetric design of a Sphere was one of the potential carrier geometries, even though a perfect Sphere might not serve as the best particle geometry, despite good flowability, as it offers a minimized surface per mass to attach drug particles. Further, the surface is maximally exposed to neighboring particles. During the mixing process, collisions between carrier particles could further press the drug particles onto the surface of the carrier, increasing the contact area and potentially impeding detachment. Therefore, three further geometries were derived from the Sphere (Fig. 1). On the Pharmacone, spikes were added. The spikes could passivate the surface and create pockets for attached drug to be sheltered from shear and press-on forces during the blending process. Furthermore, the spikes could lead to a turbulent moving and flying behavior, which could increase the dispersion forces. The Soccerball contains indentations, giving the same feature of a surface passivation and coverage for the drug. Lastly, the Rollingknot was a design aiming for a low volume to surface area ratio. With the printed particles, realistic interactive powder mixtures were blended with the model drug budesonide and analysed. Budesonide was chosen as it is one of the drugs used in interactive powder mixtures and shows quite uniform particles after micronisation. In addition to different tested complex geometries for the carrier particles, an influence of the surface roughness onto the performance was investigated. By changing printing parameters, the surface of the printed particles could be changed in a controlled manner.
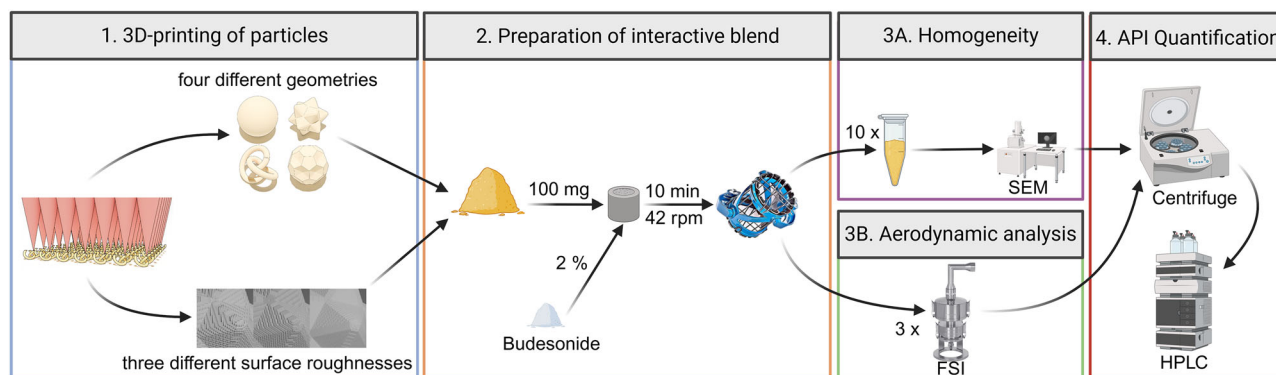
Fig. 2 | Carrier particle workflow. Beginning with 1, the 3D laser printing of four different carrier geometries and three different surface roughnesses, 2, creation of the interactive powder mixture, 3, performance testing of the powder mixture for homogeneity and aerodynamic analysis and 4, quantification of the active pharmaceutical ingredient (API) budesonide with the high-performance liquid chromatography (HPLC) after centrifugation.
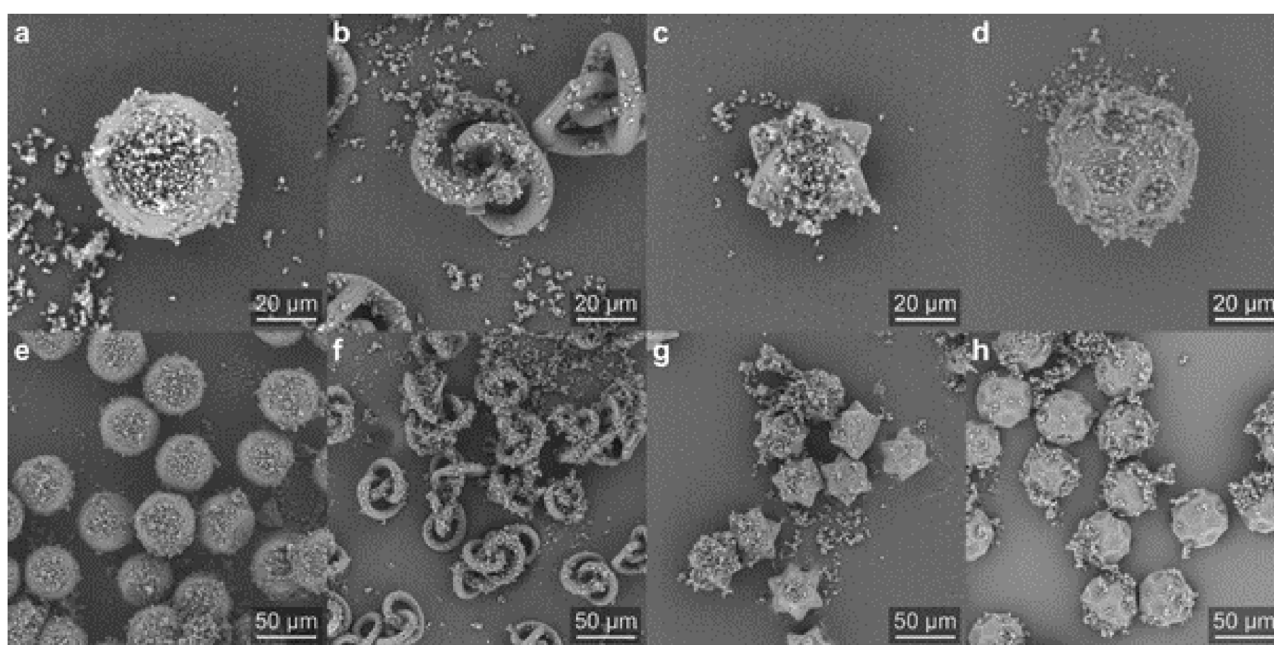
Fig. 3 | Scanning electron micrographs of interactive powder mixtures. a–d of single carrier particles after blending with 10% (w/w) of the active pharmaceutical ingredient. The images show the particle designs **a** Sphere, **b** Rollingknot, **c** Pharmacone, and **d** Soccerball. **e–h** Scanning-electron micrographs of the powder bulk after blending, showing the same particle designs.

Results

Experimental performance testing

The required carrier particles were fabricated in large quantities using multi-focus multi-photon 3D laser printing. By combining an array of $7 \times 7 = 49$ laser foci with focus scanning speeds of up to $1\,m/s$, millions of tailored carrier particles can be produced in only a few weeks[24]. By coating the substrate with a thin layer of polyvinyl alcohol (PVA) prior to printing, a damage-free lift-off procedure is possible by a subsequent immersion of the substrate in warm aqua bidest. After washing and drying, the printed particles were mixed with the API budesonide to form a stable interactive powder mixture. The powder mixture then was used for homogeneity testing and aerodynamic analysis (Fig. 2).

The created powder blends were visualised using scanning-electron microscopy (SEM). Figure 3a–d shows the images of the four geometries after mixing them with 10% API. The API is able to adhere to each of the four different carrier particle geometries. Figure 3e–h shows images of the powder bulk with a similar loading for multiple carrier particles. It is

apparent that the API not only sticks to the surface of the carrier particles but also partly tends to build API agglomerates.

Simulation and characterisation of different surface roughnesses

To study the impact of varying surface roughness, the best-performing carrier particle design, namely the Pharmacone, was printed using different hatching and slicing parameters. Figure 4 shows the resulting structures. By applying a well-described model for the multi-photon dose, the structure resulting from 3D laser printing can be simulated[31]. Incorporating the hatching and slicing parameters together with other important manufacturing conditions like, e.g., laser power or focus scanning velocity, allows for visualising the simulated structure. Figure 4a–c shows the simulated Pharmacone particles for hatching distances between 200 nm and 700 nm as well as slicing distances between 200 nm and 500 nm. By analyzing the simulated structure, an estimate for the surface area per particle can be calculated which varies between 6000 µm² and 12600 µm² and shows a clear
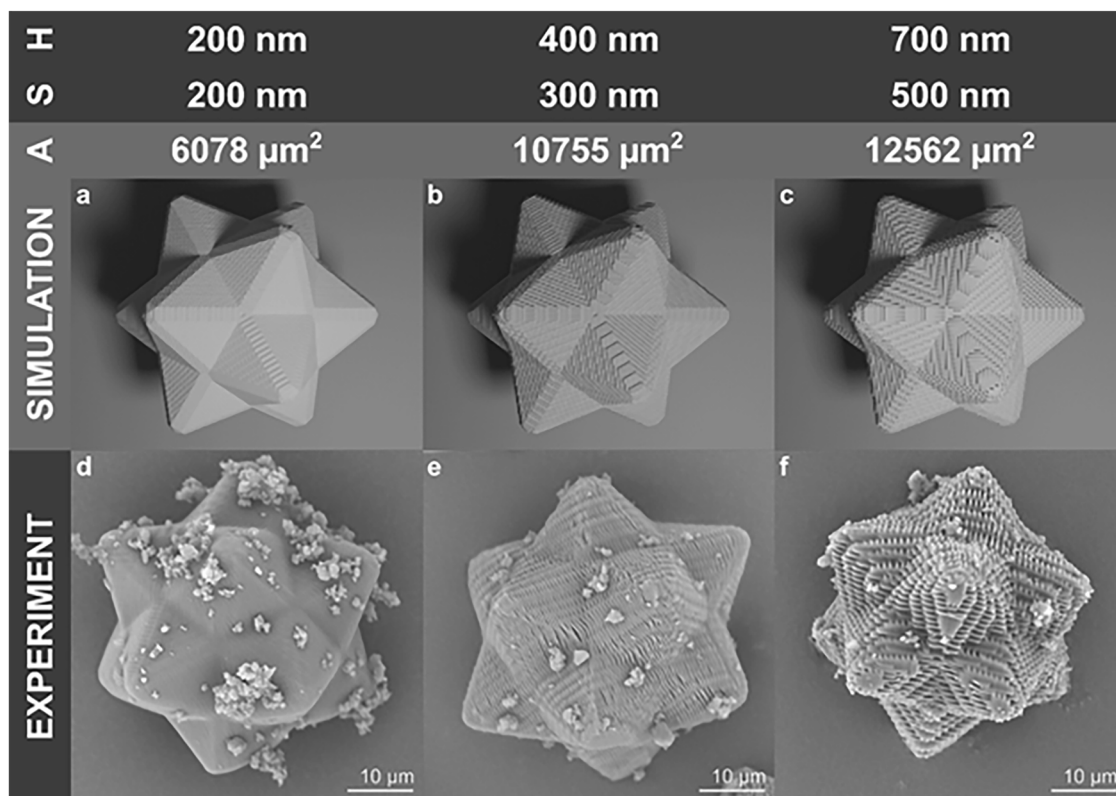
Fig. 4 | Surface roughness analysis for the printing parameters hatching (H) and slicing (S). By simulating the total exposure dose, the respective theoretical surface area (A) could be calculated. **a-c** simulated carrier particles with different hatching and slicing parameters. **d–f** scanning-electron micrographs of single carrier particles after blending with 2% (w/w) of the active pharmaceutical ingredient and labelled as **d** smooth Pharmacone, **e** medium Pharmacone, and **f** rough Pharmacone.

dependence on hatching and slicing. Figure 4d–f shows scanning-electron micrographs of Pharmacone carrier particles that were manufactured using these exact parameters to allow for comparing the simulation to the real-world experiment. While the structure appears to have a slightly higher total surface area for large hatching and slicing distances, it is clear that the variation of hatching and slicing yields the desired change in surface roughness.

Experimental performance assessment

For all six powder blends, the recovery and relative standard deviation (RSD) of the recovery in the ten randomly selected samples for homogeneity tests were calculated. The data is visualised in Fig. 5. For the recovery, the desired range was set between 90% and 110%. For the RSD, the result should be as low as possible with a maximum limit for acceptance at 15%. Sufficient API recovery is needed to demonstrate that the API is loaded onto the carrier instead of building up API agglomerates in dead zones in the corners of the mixing device. All batches with Pharmacone, except for the smooth Pharmacone that slightly exceeded the upper limit, and Sphere carrier particles led to results within the limits of the recovery. The Soccerball (recovery = 44.2%) and the Rollingknot (recovery = 72.9%) resulted in recoveries below the 90% mark indicating incomplete adhesion of API to the respective carrier. The results of the recovery coupled with the results of the relative standard deviation indicated, that the Soccerball (RSD = 45.9%) and Rollingknot (RSD = 40.6%) did not show homogeneous powder blends. All Pharmacone batches as well as the Sphere powder blend did result in RSD values below the 15% mark. Therefore, these four blends were classified as homogeneous.

For all six powder blends the aerodynamic impaction analysis was performed in triplicate. The recovery of the administered API and the fine particle fraction below 5 μm (FPF) were calculated for each impaction run. Results are shown in Fig. 6. All three types of Pharmacone carrier particles with different surface roughness as well as the Sphere carrier particles

achieved a mean recovery of the API mass in the desired limits between 90% to 110%. Nevertheless, only the Sphere performed consistently enough to show a standard deviation in between the limits as well. The Soccerball, with a small standard deviation, had its mean recovery above the limits at 112.8%. The Rollingknot showed the worst recovery; the mean value was far below the limits (70.8%), accompanied by the largest standard deviation.

No limits were placed on FPF other than it should be as high as possible. Here, a clear trend is visible when comparing the three Pharmacone structures with the other three geometries. Sphere (3.8%) and Soccerball (3.8%) performed the same, the Rollingknot (2.3%) obtained the worst mean value but did not differ significantly from the Sphere. All three Pharmacone blends did perform significantly better than the other geometries. Between the Pharmacone particles of different surface roughness, no significant difference was found (Smooth Pharmacone: 18.1%, Rough Pharmacone 17.0% and Medium Pharmacone 16.9%). Compared to the next-best powder blend, the Sphere, all Pharmacones performed significantly better.

Discussion

The SEM images visualise the adhesion behavior of the API. For a homogeneous API loading, the API should cover the carrier particles evenly with the same amount of API on all carrier particles. The images in Fig. 3 show that the API covered the carrier particles sufficiently, no large powder nests of API were found. When looking at the Sphere powder bulk, the API seemed to be evenly distributed on the single carrier as well as in between the carrier particles. The Rollingknot was less evenly covered. Some carrier particles showed almost no attached API while others appeared to be completely covered with API. The same effect, but not as prominent, was found for the Pharmacone. For the Pharmacone it was especially recognizable that the API did not only attach to the indentations between the spikes but also everywhere on the spikes. The spikes might be exposed to more stress forces during mixing which could hinder API to stay attached.
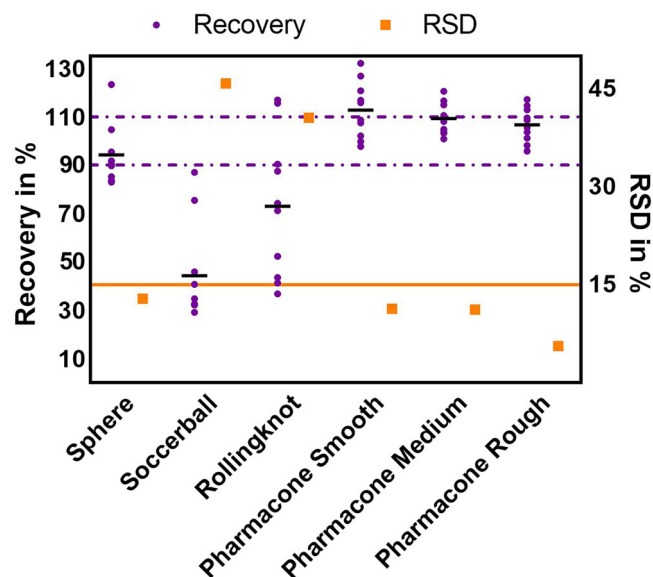
Fig. 5 | Results of homogeneity evaluation. The recovery of active pharmaceutical ingredient in % on the left vertical axis and the relative standard deviation (RSD) in % on the right vertical axis, individual data points for the recovery are shown as violet dots plus mean value with a black line and dashed lines as the upper (110%) and lower (90%) limits for the recovery, $n = 10$, data for the RSD are shown as orange squares with a continuous line for the upper limit (15%) of the RSD.
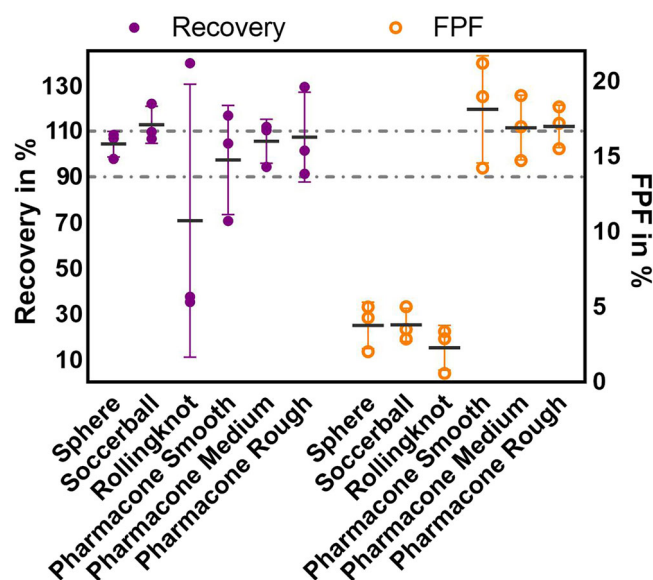
Fig. 6 | Results of aerodynamic analysis. The recovery of active pharmaceutical ingredient (API) in % plus mean value as black line on the left vertical axis and the fine particle fraction below 5 μm (FPF) in % plus mean value as black line on the right vertical axis, data for the recovery is shown in violet dots with dashed lines as the upper (110%) and lower (90%) limits for the recovery, data for the FPF is shown as orange bars, $n = 3$, error bars = standard deviation.

The Soccerball showed a good API coverage with the API primarily sticking to the flat surfaces rather than to the edges of the particle.

The interaction of the API particles with the Pharmacones is captured in the SEM images of the powder blends with the Pharmacones of different surface roughness (Fig. 4). The rougher the Pharmacones are, the deeper and broader are the grooves on their surfaces. In the pharmaceutical context a distinction is made between microroughness, if the grooves are in a size range of more than a micrometer, or nanoroughness, if the grooves are smaller than a micrometer. Thus, these grooves could have two different

effects[32]. On one side if the groove is large enough, namely microroughness dominates, API could enter the groove. This would lead to more contact points, thus more adhesive forces and a reduction in redispersion of the API during inhalation. On the other side, if the groove is too small for the API to enter, namely nanoroughness, the grooved surface would lead to less contact and adhesion points between API and carrier and thus to a higher detached fraction during inhalation. This is graphically exemplified in Fig. 7. If comparing different nanoroughnesses, hypothetically the smoother the surface, the more contact area with the API could occur, leading to higher adhesive forces and less detachment during inhalation.

The API, having a mean diameter of 1.43 μm, was larger than the largest grooves on the rough Pharmacone. Therefore, the here created differences in the surface roughness are on a level of varying nanoroughness. We observed that the API did not enter the grooves but rather attached on top of them. This might have resulted in a larger contact area between API and the smooth Pharmacone compared to the medium and rough Pharmacones.

A homogeneous powder blend is an essential prerequisite for a reliable drug administration by inhalation. The powder blends were analysed for their respective API recovery and RSD after blending. A recovery between 90% and 110% indicates that the API sufficiently adhered to the carrier particle's surface. If the adhesion is not sufficient, the API would rather stick together and build up separate agglomerates, influencing recovery and RSD. This might also be the result if the carrier particles did not build up enough kinetic energy to stir up the API powder and disperse it during mixing or if the surface coverage ratio (SCR) is too high. The SCR calculates the theoretical projected area of the drug particles in relation to the total surface area of the carrier particle. If the SCR exceeds 1, the surface is overloaded and drug particles must form agglomerates. This was not the case for any powder mixture created as the SCR was always below 0.25. Analyzing the homogeneity for the different carrier geometries shows that only the Soccerball and the Rollingknot lacked a sufficient recovery and RSD (Fig. 5). Therefore, these powder batches could not be seen as homogeneous, hence, the results of aerodynamic testing need to be interpreted with caution. For the Rollingknot, its inability to disperse the API powder bed could be regarded as the prominent cause of poor recovery, as a single Rollingknot is quite light compared to all other carrier geometries. Hence, less kinetic energy is created during mixing, affecting the mixing performance. The Rollingknot has roughly the same surface area compared to the other geometries, but the accessibility of the surface area differs. The inner sides of the knot-structure might be less accessible during mixing and thus be inferior in attaching API. Additionally, if the carrier particles stick together, the surface might not be accessible for the API. This might in particular be a problem for the Rollingknot. The single carrier particles tended to interlock with each other, building up blocks of carrier in which the API could not enter easily. The Soccerball has the largest surface area per particle of all printed particles. Nevertheless, the recovery is below the set limit. The cavities on the Soccerball did not have the positive effect expected, which was to store and protect the API from heavy press-on forces and irreversible attachment during mixing. Apparently, either the API did not attach to the Soccerball in the first place or was shoved off and did not get reattached again during mixing. On the other side, especially the Pharmacone with its spikes could provide extraordinary shear forces leading to a better agglomerate break-up and thus a better homogeneity. Comparing the recovery of the three different surface roughnesses, a slight but not significant trend is visible. From the smooth to the rough Pharmacone, the recovery increased aligning with the increased surface area (Fig. 4) due to the increased surface roughness. This could be interpreted in terms of a better attachment to the rough Pharmacone. However, as explained before, the increased roughness on the nanoscale does not create a larger potentially accessible surface area for the API, which is larger by an order of magnitude. For a further understanding, more experiments are needed.

It needs to be addressed that the blending protocol used in this study was limited by the number of printed particles. A thorough blending optimization could not be performed, therefore a standard protocol, sufficient
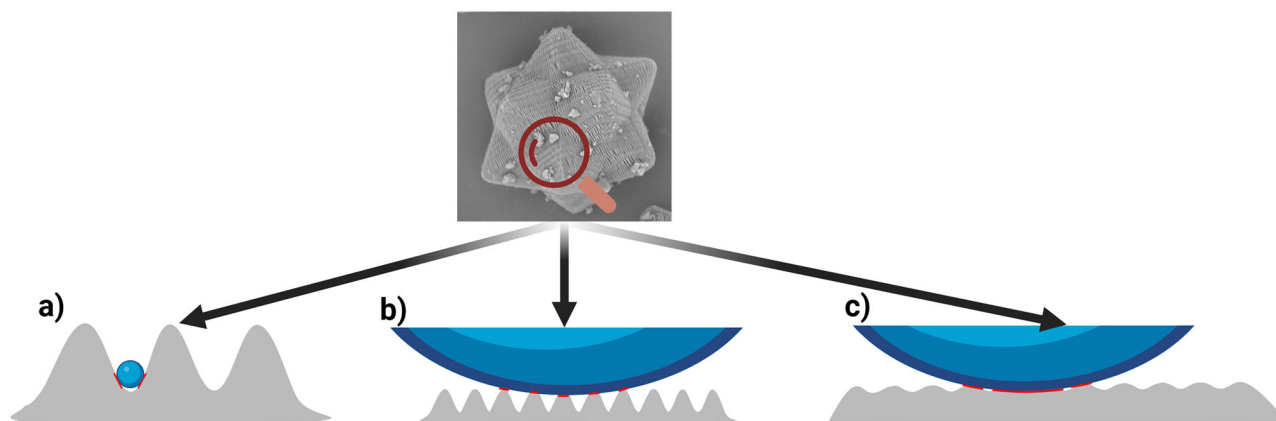
Fig. 7 | Surface interaction of carrier (gray) with active pharmaceutical ingredient (API) (blue). a Surface grooves of carrier are larger than API leading to API getting stuck; **b** API is larger than grooves, rough surface leading to small contact area; **c** API is larger than grooves, smooth surface leading to larger contact area.

for creating homogeneous powder blends, was used for all mixtures to provide a fair comparison. Nevertheless, with an optimized blending process, even the Rollingknot and the Soccerball could potentially achieve homogeneous powder blends.

The impaction analysis represents the most important aspect of the performance characterization for the powder blends. Only aerosolized API, measured as an FPF, can later be inhaled to the lungs and have the intended pharmacologic effect. The insufficient recovery during the impaction analysis of the Soccerball and the Rollingknot could be explained by the respective recovery and RSD in the homogeneity testing. If the powder batch is not homogeneous, the loaded powder in the inhaler cannot be precisely correlated to a calculated mass of API. Even though the theoretical mass of API loaded into the inhaler was calculated with the detected mean percentage of API in the powder blend, the actual percentage in the used sample might differ. Thus, the theoretical mass of API per inhalation and the actual recovered mass of API per inhalation can have higher discrepancies.

The Pharmacone with its significantly higher FPF compared to the other three geometries, showed to be the superior carrier particle geometry. The better dispersion of API is probably due to the aerodynamic flying behavior of the carrier particles. In the literature, three main mechanisms are known for the redispersion of the API in the air flow (Fig. 8)[33]. The shear forces of the surrounding air can directly lift off the API particles from the surface. Due to inertia, the carrier particles are traveling through the inhaler device slower than the surrounding air. Additionally, the API particles are lighter than the carrier, resulting in less inertial retention. Due to the relative motion and velocity gradient between drug and carrier, drug particles can lift off of the carrier's surface following the air stream and overcoming the adhesive forces. Nevertheless, the extent of API lift off is dependent on the accessibility of the API to the air flow. On the surface of the Soccerball, the API might be stored in the indentations, sheltered from bypassing air. An important factor for detachment might also be the extent of contact area and attachment between API and carrier. The contact area between API and carrier is highly dependent on the mechanism of press-on forces during mixing[34]. On the surface of the Sphere, the API is not sheltered from press-on forces during the mixing process, which could lead to an inferior detachment. This would be different for the other geometries, where the spikes or indentations would shelter API from the press-on forces.

The second and third mechanism for detachment, as shown, are collisions of the carrier particles, either with other carrier particles or with the walls of the inhaler device. Additionally, the impact forces and the flying behavior of the particles might be of major influence. The impact force during collision correlates with the velocity and the mass of the impacting particle. The velocity is mainly defined by the air stream which was set equal

for all particles. The mass of the carrier particle on the other side differs significantly for the Rollingknot. The mass of a single Rollingknot particle is five-fold smaller than that of the Soccerball (Fig. 1). This directly correlates to an inferior impact force and thus less detachment of the Rollingknot. API dispersion is also dependent on particle movement, i.e., linear or chaotic flying behavior. Turbulences, introducing shear and centrifugal forces, increase the detachment. Additionally, a turbulent movement would consequently lead to more collisions in total. The more linear the particle moves through the inhaler device, the lower is the likelihood of collisions. The Sphere on one side would not go into a turbulent movement neither at collision nor during free flying. As known for spherical objects colliding with a wall, the angle of incidence equals the angle of reflection[35]. On the other side, the Phamacone's surface spikes lead to an uncontrolled spinning of the particle after collision (data not shown). The same effect occurs for the other two geometries, Soccerball and Rollingknot, but to a lesser extent. This behavior during collisions might be the most prominent factor why the Pharmacone showed the best results in the impaction analysis. While the geometry of the carrier did show an influence, the varied nanoroughness of the carrier's surface did not affect the performance. As explained before, differences in roughness may change contact area and thus lead to an easier detachment. This could not be shown here. The trend of the standard deviation between the three Pharmacones might indicate a more constant performance with a higher surface nanoroughness.

While the FPFs reported in this study appear to be low, compared to current commercial products, it needs to be stressed that this is due to the used device. With the same device, the gold standard of lactose carrier particles (Supplementary Table 1) did show comparably low FPFs as visualised in the Supplementary Fig. 1.

In this study, only one model drug, budesonide, was tested. Furthermore, the FSI does not allow for a full analysis of the aerodynamic particle size distribution (APSD) of detached drug. With regard to the drug, the cohesive-adhesive-balance (CAB) between drug and carrier particles has a well-studied critical impact on the FPF. A higher cohesiveness of the drug rises agglomeration tendencies resulting in drug-agglomerates with an aerodynamic diameter above 5 μm if the dispersion forces during inhalation are not strong enough, while a higher adhesiveness of drug to the carrier would hinder the overall detachment of drug from its carrier. While in this study only budesonide was used, the CAB between the drug and all carrier particles was identical as the same polymer was used for the printing. Agglomerate formation was minimized with a small drug-carrier ratio, as explained above with the SCR[36]. Nevertheless, other drugs with a differing CAB as well as other drug particle morphologies could result in a different outcome for the FPF. As the same drug particle size distribution was used for all interactive blends, the

Fig. 8 | Detachment mechanisms for the active pharmaceutical ingredient (API) during the inhalation process. a by shear forces of the surrounding air flow (velocity gradient indicated by color gradient); **b** by particle-particle collisions between two coarse carrier particles; **c** by particle-wall collisions of a carrier particle with the inhaler device.
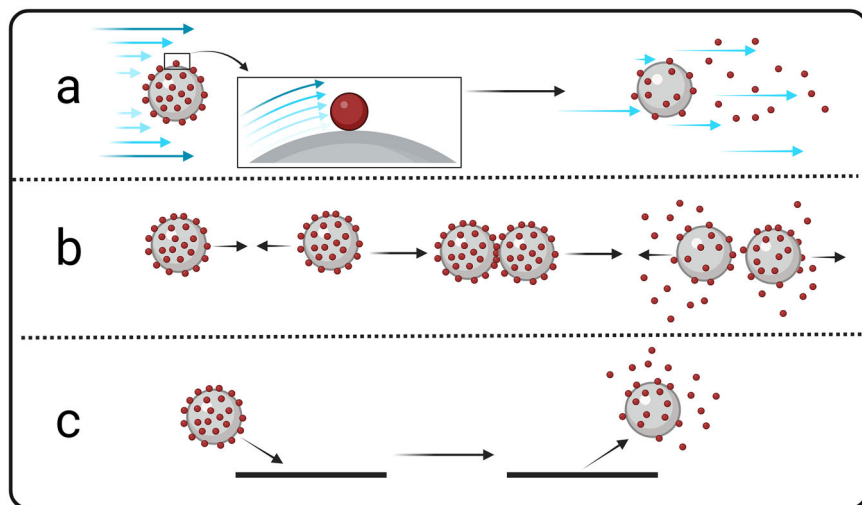
APSD could be influenced by agglomeration tendencies and the dispersive forces in the device. While the former was kept small, the latter is highly dependent on the device itself. The here used Rack device (Supplementary Fig. 2) was chosen to keep intrinsic dispersion forces small, reducing the visible effect on the carrier geometry. Therefore, the difference in APSD was estimated to be small in this setup.

Conclusion

Using the latest generation of rapid multi-photon multi-focus 3D laser printing, we systematically investigated the effect of geometry on the aerodynamic performance of tailor-made carrier particles for inhalation in this study. We were able to produce millions of highly resolved uniform complex carrier particles of four different geometries and three different surface roughnesses within a few weeks of print time. With two carrier particle geometries, namely the Sphere and the Pharmacone and the latter one in three different surface roughnesses, respectively, it was possible to create homogeneous powder blends. In the aerodynamic assessment, the Pharmacone outperformed the other geometries significantly. The unique feature in the design of the Pharmacone geometry are the surface spikes (Fig. 1). These spikes are responsible for the good performance at creating a homogeneous powder blend as well as during the aerodynamic assessment. Therefore, an influence of the carrier geometry on the performance during inhalation was proven. As the Pharmacone was primarily identified as the best of the four geometries, it was used as the geometry for different surface roughnesses. The difference in surface roughness was on the nanoscale, smaller than the API particles that attach to the surface of the carrier particle. The results from the homogeneity test as well as the impaction analysis showed no significant differences between the Pharmacones. Therefore, an influence of the nanoroughness of the carrier particle could not be identified in this study.

Taken together, tailor-made carrier particles for interactive powder mixtures can be produced by laser-based additive manufacturing techniques and result in homogeneous powder blends with API. While the additively manufactured carrier particles are not meant to be used as an actual inhaled product in their current form and amount, the method allows the fabrication of large amounts of particles to investigate the influence of carrier particle geometry and nano-roughness on its performance in carrier-based inhalation powder blends. While the geometry of the carrier particle clearly did influence the performance, the alteration of nano-roughness did not. The Pharmacone geometry is the most promising candidate for further testing especially in the context of parametric design to find the optimal geometry for the carrier particle in the next generation interactive powder mixture for drug delivery to the lungs.

Experimental Section/Methods

Multi-focus 3D-laser-printing setup

The setup used for multi-photon multi-focus 3D laser printing of large numbers of carrier particles was already described elsewhere[24]. The output of a mode-locked laser (790 nm center wavelength, 3.7 W average power, 80 MHz repetition frequency, 140 fs impulse duration; Coherent Chameleon Ultra II) is relayed on a diffractive optical element and a multi-lens array to generate a $7 \times 7 = 49$ focus array. By using galvanometric mirrors and a 40x/NA1.4 objective lens (Carl Zeiss), this focus array is scanned laterally with a focus velocity of $v = 1 \frac{m}{s}$. This setup has been described in detail previously[24].

Used photoresist

For printing, a photoresist containing 0.5% (w/w) BBK[31] is used in the monomer mixture IP-Dip NPI (IP-Dip without photoinitiator obtained from Nanoscribe GmbH).

Sacrificial layer

To allow for a damage-free lift-off procedure, the target structures were printed on a sacrificial layer based on 7% (w/w) polyvinyl alcohol (PVA) in water that was created by spin coating (KL-SCE-150, Quantum Design GmbH) with 67rps for 60s and subsequent hot-plate baking at a temperature of 80 °C for 2min.

Development of particles

After printing, the substrate was developed for 2 times 10 minutes in 1-methoxy-2-propanyl acetate (PGMEA), followed by 2 times 5 minutes in Isopropanol and left to dry.

Different roughnesses

To vary the surface roughness of the carrier particles, different hatching and slicing distances, varying between 200 nm and 700 nm (see Fig. 4), were chosen.

Particle surface simulation

By calculating the multi-photon exposure dose of each structure[31], the expected shape after manufacturing was simulated. Using the software Blender (Blender Foundation), the surface area and mass of each particle was calculated based on this simulation.

Preparation of powder blends

For each printed carrier particle type, a powder blend was produced. As a model API Budesonide (AM02-00049, Minakem, France) was used. The mean particle size of the model API was measured to be 1.43 µm with a span

value of 1.99 (HELOS, Sympatec GmbH, Germany, laser diffraction, 4 bar dispersion pressure). The budesonide was mainly crystalline (Supplementary Fig. 3) as analysed with dynamic vapor sorption (Supplementary Method 1). As a mixing vessel, a custom-made aluminum vessel with a maximal filling volume of 2 ml was manufactured. The inner corners were rounded, and the lid was placed and fixed on the vessel without a thread in a manner to reduce the attachment of API and the accumulation of powder nests. First, the printed carrier particles were weighted in. This resulted in 57 mg for the Soccerball, 68 mg for the rough Pharmacone, 82 mg for the medium Pharmacone, 93 mg for the smooth Pharmacone, 5 mg for the Rollingknot and 62 mg for the Sphere. API was weighted on top, making up 2% (w/w) of the total powder mass. The mixing vessel was filled to around 30% of its maximal filling volume.

Mixing was performed with a Turbula Mixer® (WAB-Group, Switzerland) at 42 rpm for 10 minutes.

In total, six different powder blends were produced, namely Sphere, Soccerball, Rollingknot, Pharmacone smooth, Pharmacone medium and Pharmacone rough.

Additionally, four powder blends with an API content of 10% (w/w) were created in the same manner that were solely used for scanning electron microscopy images. The Rollingknot particle had to be treated differently. Due to its small volume compared to the other particles, the same number of particles resulted in a much smaller mass. Nevertheless, the Rollingknot particle had around the same surface area per particle and thus roughly the same total surface area as the other geometries (Fig. 1). Therefore, the API content was raised to 40%, which was the same absolute mass of API as for the other geometries, to ensure a comparability and a sufficient API amount for later analysis. With the higher content, a better idea of the accessibility of the different surfaces of the complex geometries and the attachment of fine API could be gained.

Powder content homogeneity

To assess the homogeneity of the API content in the powder blend, ten samples were drawn from the mixed powder. Therefore, the entire amount of powder was evenly spread in a Petri dish to form a flat powder bed. For each sample it was ensured that the full depth of the powder bed was included. The locations of the samples were evenly distributed over the whole Petri dish with even distances to representatively cover the entire powder layer. Each sample was around 5 mg, weighed in at an accuracy of 0.001 mg. The samples were dissolved in 1.0 ml ethanol. To separate the printed particles from the dissolved API, the samples were centrifuged for 10 min at 14000 rpm in a Centrifuge 5430 R (Eppendorf SE, Hamburg, Germany). 400 µl of the supernatant liquid were diluted to 2.0 ml with ethanol and used for analysis. As marker for the powder homogeneity the API recovery in the ten samples relative to the supposed 2% (w/w) and the RSD of the former were assessed. API recovery was supposed to be in between the error margins of 100% ± 10%. Due to the miniature method of the well-studied low shear blending of interactive powder mixtures in the Turbula Mixer® and the associated difficulties in the handling of such small amounts of powder blends, the limit for the RSD was raised to <15%.

Impaction analysis

The impaction analysis was performed with the Fast Screening Impactor (FSI, Copley Scientific Ltd., Nottingham, United Kingdom). As device the Rack[37,38] (Supplementary Fig. 2) was used, which allows application of powder to the inhalation airflow without additional dispersion effects from the device. The cut-off for the fine particle fraction was set at 5 µm with a flow rate of 80 l/min correlating to a pressure drop of 4 kPa, according to the Ph. Eur. guideline for Inhalanda. The inhalation process lasted for 3.1 s resulting in a total inhalation volume of 4 l. For each of the six carrier geometries, impaction analysis was performed as a triplicate with three individual doses per analysis. For a single dose, 10 mg of powder blend were metered into an Eppendorf tube and directly loaded into the Rack. API collection from the four stages, namely device plus Eppendorf tube, throat plus mouthpiece, coarse particles in the pre-separator and fine particles on

the filter, was performed by dissolving the API in 10 ml ethanol per stage. After quantification of API, the FPF was calculated. This was the amount of API found on the filter stage, representing the particles below 5 µm in aerodynamic diameter, divided by the total amount of API that was delivered from the device and recovered during analysis. Additionally, the recovery of API in the analysis was calculated. For that, the total amount of recovered API was compared to the loaded amount of API into the device as calculated from loaded powder mass and determined API concentration of the blend.

API quantification

The quantification of API in the powder blends as well as in the collected stages of the impaction analysis was performed by high performance liquid chromatography (HPLC) with an Alliance HPLC-System equipped with an UV/Vis detector (Waters Corporation, Milford, United States) measurements. As a stationary phase, a Lichrospher® 100 RP-18 5 µm (Merck, Darmstadt, Germany) column was used. As a mobile phase an in-device mixture of 75% methanol in HPLC grade provided by J. T. Baker (Pennsylvania, USA) and 25% aqua bidest. was used. The samples of the impaction analysis were centrifuged for 10 minutes at 14000 rpm in a Centrifuge 5430 R (Eppendorf SE, Hamburg, Germany) to separate the insoluble carrier particles from the API solution. The supernatant was used for quantification. The homogeneity samples of the dissolved powder blends were analysed after dilution.

The HPLC method was validated covering specificity, precision and reproducibility. The limit of quantification (LOQ) and limit of detection (LOD) for the method were calculated according to the ICH guideline[39], based on the standard deviation method. The LOQ was calculated to be 0.045 µg/ml and LOD 0.015 µg/ml.

Quantification of the API content was done by using an external standard calibration. The calibration covered an API concentration range of 1 – 100 µg/ml ($R^2 > 0.99$), all observed samples were within this range.

Scanning electron microscopy

The printed particles as well as the produced powder blends were visualised using scanning electron microscopy (SEM). The powder blends were visualised using a Phenom XL (Phenom-World BV, Eindhoven, The Netherlands). Image acquisition was done with the compatible Phenom ProSuite Desktop SEM Software. The samples were adhered to aluminum stubs using carbon stickers (Plano GmbH, Wetzlar, Germany). The samples were gold sputtered prior to visualisation using a BAL-Tec SCP 050 Sputter Coater (Leica Instruments, Wetzlar, Germany). Individual particles and powder nests were analysed at different magnitudes, specified in the description of the images. For the comparison of the different geometries, the powder blends with 10% API were used, for the comparison of the different surface roughnesses, the powder blends with 2% were used. With fewer API particles on the surface, the interaction of single API molecules with the cavities on the carrier surfaces were better visible.

References

1. Sanders, M. Pulmonary Drug Delivery: An Historical Overview. In Controlled Pulmonary Drug Delivery, edited by H. D. Smyth & A. J. Hickey (Springer New York, New York, NY, pp. 51–73, (2011).
2. Patil, J. S. & Sarasija, S. Pulmonary drug delivery strategies: a concise, systematic review. *Lung India* **29**, 44–49 (2012).
3. Newman, S. P. Dry powder inhalers for optimal drug delivery. *Expert Opin. Biol. Ther.* **4**, 23–33 (2004).

4. Clark, A. R. Half a Century of Technological Advances in Pulmonary Drug Delivery: A Personal Perspective. *Front. Drug Delivery* **2** https://doi.org/10.3389/fddev.2022.871147 (2022).

5. Lavorini, F. et al. Retail sales of inhalation devices in European countries: so much for a global policy. *Respir. Med.* **105**, 1099–1103 (2011).

6. Lumb et al. Nunn and Lumb's Applied Respiratory Physiology, Ninth Edition. Chapter 1 - Functional anatomy of the respiratory tract. 9th ed. (Elsevier, 2020).

7. Labiris, N. R. & Dolovich, M. B. Pulmonary drug delivery. Part I: physiological factors affecting therapeutic effectiveness of aerosolized medications. *Br. J. Clin. Pharmacol.* **56**, 588–599 (2003).

8. Daniher, D. I. & Zhu, J. Dry powder platform for pulmonary drug delivery. *Particuology* **6**, 225–238 (2008).

9. Chaurasiya, B. & Zhao, Y.-Y. Dry Powder for Pulmonary Delivery: A Comprehensive Review. *Pharmaceutics* **13**; https://doi.org/10.3390/pharmaceutics13010031 (2020).

10. Boer, A., de, Gjaltema, D., Hagedoorn, P. & Frijlink, H. Characterization of inhalation aerosols: a critical evaluation of cascade impactor analysis and laser diffraction technique. *Int. J. Pharm.* **249**, 219–231 (2002).

11. Kassinos, S., Bäckman, P., Conway, J., Hickey, A. J. Inhaled Medicines (Elsevier, 2021).

12. Smyth, H. D. & Hickey, A. Carriers in Drug Powder Delivery. Implications for Inhalation System Design. *Am. J. Drug Delivery*, 117–132 (2005).

13. Tong, Z. B. Discrete modelling of powder dispersion in dry powder inhalers - a brief review. *Curr. Pharm. Des.* **21**, 3966–3973 (2015).

14. Taburet, A. M. & Schmit, B. Pharmacokinetic optimisation of asthma treatment. *Clin. Pharmacokinet.* **26**, 396–418 (1994).

15. Zellnitz, S. et al. The Importance of Interactions Between Carrier and Drug Particles for the Application in Dry Powder Inhalers. In Particles in Contact, edited by S. Antonyuk (Springer International Publishing, Cham, pp. 457–516 (2019).

16. S. Edge, P. M. Young, R. Price, M. J. Tobyn, S. Kaerger. Carriers for DPIs: formulation and regulatory challenges. Pharmaceutical Technology Europe 2006 (2006).

17. Kou, X., Chan, L. W., Steckel, H. & Heng, P. W. S. Physico-chemical aspects of lactose for inhalation. *Adv. Drug Deliv. Rev.* **64**, 220–232 (2012).

18. Zellnitz, S., Redlinger-Pohn, J. D., Kappl, M., Schroettner, H. & Urbanetz, N. A. Preparation and characterization of physically modified glass beads used as model carriers in dry powder inhalers. *Int. J. Pharm.* **447**, 132–138 (2013).

19. Renner, N., Steckel, H., Urbanetz, N. & Scherließ, R. Nano- and Microstructured model carrier surfaces to alter dry powder inhaler performance. *Int. J. Pharm.* **518**, 20–28 (2017).

20. Garcia, A. et al. Microfabricated engineered particle systems for respiratory drug delivery and other pharmaceutical applications. *Journal of drug delivery* **2012**, 941243 (2012).

21. Hassan, M. S. & Lau, R. Feasibility study of pollen-shape drug carriers in dry powder inhalation. *Journal of pharmaceutical sciences* **99**, 1309–1321 (2010).

22. Varun, N. & Ghoroi, C. Crystallization induced flower-like lactose as potential carriers for dry powder inhaler application. *Powder Technol* **403**, 117391 (2022).

23. Bock, S., Rades, T., Rantanen, J. & Scherließ, R. Additive manufacturing in respiratory sciences - Current applications and future prospects. *Adv. Drug Deliv. Rev.* **186**, 114341 (2022).

24. Kiefer, P. et al. A multi-photon (7 × 7)-focus 3D laser printer based on a 3D-printed diffractive optical element and a 3D-printed multi-lens array. *Light Adv. Manuf.* **4**, 28–41 (2024).

25. Fladung, M. et al. What lies beyond—Insights into elastic microscaffolds with metamaterial properties for cell studies. *Curr. Opin. Biomed. Eng.* **33**, S. 100568 (2025).

26. Somers, P., Koch, S., Kiefer, P., Meretska, M. L. & Wegener, M. Holographic multi-photon 3D laser nanoprinting – at the speed of light: opinion. *Opt. Mater. Express* **14**, S. 2370 (2024).

27. Scherließ, R. & Bock, S. Pulverförmige Formulierungen zur Inhalation. Offenlegungsschrift (2019).

28. Wostry, M. & Scherließ, R. In-silico evaluation of different carrier particle geometries in interactive powder mixtures. Drug Delivery to the Lungs (2023).

29. Wostry, M. & Scherließ, R. Customised carrier geometries for inhalation – from in-silico experiments to 3D-printed particles. Drug Delivery to the Lungs (2024).

30. Wostry, M. & Scherließ, R. Possibilities and advantages of additive manufacturing in dry powder formulations for inhalation. *Eur. J. Pharm. Sci.* **190**, 106583 (2023).

31. Kiefer, P. et al. Sensitive Photoresists for Rapid Multiphoton 3D Laser Micro- and Nanoprinting. *Adv. Opt. Mater.* **8**, 2000895 (2020).

32. Podczeck, F. Particle-particle adhesion in pharmaceutical powder handling (Imperial College Press; Distributed by World Scientific Pub, London, River Edge, NJ, 1998).

33. van Wachem, B., Thalberg, K., Remmelgas, J. & Niklasson-Björn, I. Simulation of dry powder inhalers. *Combining micro-scale, meso-scale and macro-scale modeling. AIChE J.* **63**, 501–516 (2017).

34. Thalberg, K. New theory to explain the effect of lactose fines on the performance of adhesive mixtures for inhalation. *Int. J. Pharm.* **663**, 124549 (2024).

35. Ariane, M., Sommerfeld, M. & Alexiadis, A. Wall collision and drug-carrier detachment in dry powder inhalers. Using DEM to devise a sub-scale model for CFD calculations. *Powder Technol* **334**, 65–75 (2018).

36. Ruden, J. et al. Linking carrier morphology to the powder mechanics of adhesive mixtures for dry powder inhalers via a blend-state model. *Int. J. Pharm.* **561**, 148–160 (2019).

37. Aziz, S., Scherließ, R. & Steckel, H. Development of High Dose Oseltamivir Phosphate Dry Powder for Inhalation Therapy in Viral Pneumonia. *Pharmaceutics* **12** https://doi.org/10.3390/pharmaceutics12121154 (2020).

38. Steckel, H. & Bolzen, N. Alternative sugars as potential carriers for dry powder inhalations. *Int. J. Pharm.* **270**, 297–306 (2004).

39. European Medicines Agency. ICH Topic Q2 (R1). Validation of analytical Procedures: Text and Methodology (1995).

Acknowledgements

Author contributions

Melvin Wostry (Conceptualization: Equal; Formal analysis: Lead; Investigation: Equal; Methodology: Equal; Visualisation: Equal; Writing—original draft: Equal; Writing—review & editing: Equal). Alexander Berkes (Conceptualization: Equal; Formal analysis: Supporting; Investigation: Equal; Methodology: Equal; Visualisation: Equal; Writing—original draft: Equal; Writing—review & editing: Equal). Pascal Kiefer (Conceptualization: Equal; Investigation: Supporting; Methodology: Supporting; Visualisation: Supporting; Writing—original draft: Supporting; Writing—review & editing: Equal). Martin Wegener (Conceptualization: Equal; Funding acquisition: Equal; Project administration: Equal; Supervision: Equal; Writing—review & editing: Equal). Regina Scherließ (Conceptualization: Equal; Funding

acquisition: Equal; Project administration: Equal; Supervision: Equal; Writing —review & editing: Equal).

Competing interests
The authors declare no competing interests.

Additional information
Supplementary information The online version contains supplementary material available at https://doi.org/10.1038/s43246-025-00913-0.

Correspondence and requests for materials should be addressed to Regina Scherließ.

Peer review information *Communications Materials* thanks Andrew R. Clark, Carlos A. García-González, Shadabul Haque and the other, anonymous, reviewer(s) for their contribution to the peer review of this work. Primary Handling Editors: Jet-Sing Lee. [A peer review file is available].

Reprints and permissions information is available at http://www.nature.com/reprints

Publisher's note Springer Nature remains neutral with regard to jurisdictional claims in published maps and institutional affiliations.